Impact of Two Plumes' Interaction on Submarine Melting of Tidewater Glaciers: A Laboratory Study

CLAUDIA CENEDESE

Physical Oceanography Department, Woods Hole Oceanographic Institution, Woods Hole, Massachusetts

V. MARCO GATTO

Department of Hydraulic Engineering, Delft University of Technology, Delft, Netherlands

(Manuscript received 3 September 2015, in final form 14 December 2015)

ABSTRACT

Idealized laboratory experiments investigate the glacier–ocean boundary dynamics near a vertical glacier in a two-layer stratified fluid. Discharge of meltwater runoff at the base of the glacier (subglacial discharge) enhances submarine melting. In the laboratory, the effect of multiple sources of subglacial discharge is simulated by introducing freshwater at freezing temperature from two point sources at the base of an ice block representing the glacier. The buoyant plumes of cold meltwater and subglacial discharge water entrain warm ambient water, rise vertically, and interact within a layer of depth H_2 if the distance between the sources x_0 is smaller than $H_2\alpha/0.35$, where α is the entrainment constant. The plume water detaches from the glacier face at the interface between the two layers and/or at the free surface, as confirmed by previous numerical studies and field observations. A plume model is used to explain the observed nonmonotonic dependence of submarine melting on the sources' separation. The distance between the two sources influences the entrainment of warm water in the plumes and consequently the amount of submarine melting and the final location of the meltwater within the water column. Two interacting plumes located very close together are observed to melt approximately half as much as two independent plumes. The inclusion, or parameterization, of the dynamics regulating multiple plumes' interaction is therefore necessary for a correct estimate of submarine melting. Hence, the distribution and number of sources of subglacial discharge may play an important role in glacial melt rates and fjord stratification and circulation.

1. Introduction

In the past two decades the mass loss from the Greenland Ice Sheet (GrIS) has increased and now accounts for one-quarter of global sea level rise (Shepherd et al. 2012; Church et al. 2011). Approximately half of this mass loss is tied to the speed up, thinning, and retreating of multiple marine-terminating glaciers in southeast and western Greenland that began in the mid-1990s (Rignot and Kanagaratnam 2006; Howat et al. 2007). Observations indicate that the glaciers responded to a change at their marine termini, and increasing evidence points to an increase in submarine melting at the glacier–ocean interface as a potential trigger (Vieli and Nick 2011; Straneo et al. 2013). This is consistent with the observed atmospheric and oceanic warming around Greenland that began in the mid-1990s [see review by Straneo and Heimbach (2013)].

The persistent ice loss from Greenland is also responsible for an anomalous freshwater input into the North Atlantic (Bamber et al. 2012). The implication is that GrIS mass loss may soon impact the Atlantic meridional overturning circulation and must be taken into consideration in studies of climate variability on decadal to centennial time scales. Glacier–ocean interactions thus emerge as an important potential amplifier in the context of climate change and variability [see Straneo and Cenedese (2015) for a review].

Submarine melting at the glacier terminus may impart stress perturbations and drive dynamic glacier retreat through thinning-induced ungrounding or through increased calving (Vieli and Nick 2011; O'Leary and Christoffersen 2013). There are no direct measurements

Corresponding author address: Claudia Cenedese, Physical Oceanography Department, Woods Hole Oceanographic Institution, 360 Woods Hole Road, Woods Hole, MA 02543.
E-mail: ccenedese@whoi.edu

DOI: 10.1175/JPO-D-15-0171.1

© 2016 American Meteorological Society

of submarine melting but observations from several fjords show that 1) the export of meltwaters is affected by fjord stratification (Straneo et al. 2011; Mortensen et al. 2011, 2013), and 2) localized discharge at the base of the glacier of surface meltwater (henceforward subglacial discharge) gives rise to large asymmetries in the velocity fields at the glacier edge (Motyka et al. 2013; Bartholomaus et al. 2013). This evidence suggests that submarine melting is strongly influenced by both the fjord stratification and the distribution of subglacial discharge.

Recent idealized model studies have begun to unravel the role of ocean properties, stratification, and increased subglacial discharge in setting submarine melt distribution and magnitudes (Jenkins 2011; Xu et al. 2012, 2013; Sciascia et al. 2013, 2014; Motyka et al. 2011, 2013). These models often rely on parameterizations of unresolved and poorly understood process, that is, ice–ocean boundary layer and melting of the ice front, and submarine melting is highly sensitive to the parameterizations employed. The number of sources of subglacial discharge and their distribution has been found to influence the submarine melting in recent numerical studies (Kimura et al. 2014; Slater et al. 2015; Carroll et al. 2015). To date, however, no widely applicable relationships express melt rate magnitudes and distribution as a function of subglacial discharge distribution, fjord topography and size, and/or stratification.

The current paper presents the first laboratory experiments investigating the influence of multiple sources of subglacial discharge on the submarine melting of an ice face. We restrict our attention to the subglacial discharge exiting from two sources having the same volume flux Q_{sg}, which we kept fixed, and separated by a distance x_0, which we varied. The laboratory results suggest a nonmonotonic dependence of the melt rate for small x_0 and an increase of melt rate with increasing x_0 for large x_0. We explain this behavior using the plume's idealized self-similar solutions introduced by Morton et al. (1956) and the entrainment into two interacting plumes introduced by Cenedese and Linden (2014).

2. Experimental apparatus

The description of the experimental apparatus is similar to that of Sciascia et al. (2014) as follows in the next two paragraphs. The laboratory experiments were conducted in a cold room with temperature T_{air}. During each experiment T_{air} was kept approximately constant but its value changed between experiments and ranged between 2.4° and 3.4°C. The fjord was represented by a rectangular tank, 150 cm long, 15 cm wide, and 30 cm deep (Fig. 1) that was insulated using triple-paned glass filled with argon. A

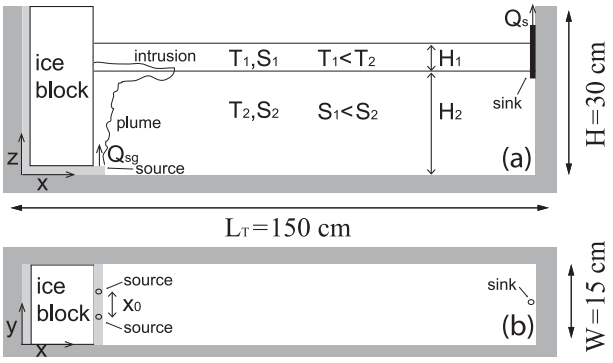

FIG. 1. Laboratory experimental apparatus: (a) side view and (b) top view. Light gray indicates the L-shaped plastic container that was used to store the plastic tubes delivering the subglacial discharge below the ice block. Sources are separated by a distance x_0, and the subglacial discharge is Q_{sg}. The same volume flux is withdrawn on the right side of the tank to keep the volume in the tank fixed. Not to scale.

two-layer stratification was produced in the tank by first adding a bottom layer of thickness $H_2' = 20.5$ cm of warmer ($T_2 \approx 3$°C), saltier ($S_2 \approx 34$ psu) water, where the prime indicates layer thicknesses before the ice block is immersed in the tank. When residual motion vanished in the bottom layer, cooler ($T_1 \approx 0.5$°C), fresher ($S_1 \approx 32$ psu) water was added from a reservoir through a float to form a second layer of thickness $H_1' = 5$ cm. The total water depth in the tank was $H_T' = 25.5$ cm. The ratio of the thicknesses of the two layers and their temperatures and salinities were chosen to approximately match those observed in winter in Sermilik Fjord (Straneo et al. 2010). Although subglacial discharge is expected to play a larger role during summer, the summer stratification is more complex (Straneo et al. 2011) and, for simplicity, we used the two-layer stratification observed in winter. The experiment began after the decay of any residual motion in the two layers.

The glacier was represented by a degassed and dyed (blue) ice block ($L_i = 10$ cm, $W_i = 15$ cm, and $H_i = 30$ cm) positioned at one end of the tank (Fig. 1). The temperature of the ice at the beginning of the experiment was $T_i \approx -25$°C, and within approximately 1 h from positioning the ice block in the tank it reached a constant value $T_i \approx -1.6$°C. The ice block was immersed very gently into the stratified water to minimize the amount of mixing between the two layers and any residual motion. The pump supplying subglacial discharge water and the pump withdrawing water at the mouth of the fjord to keep the water level constant were then started within 2 to 5 min. After the ice block was immersed in the tank, the total water depth was $H_T = 27$ cm, and the bottom and top layer thicknesses were $H_2 = 21.7$ cm and $H_1 = 5.3$ cm, respectively. The ice block was positioned on an L-shaped plastic container that stored the plastic tubes delivering the subglacial

discharge to the sources (of diameter $d = 0.22$ cm), facing vertically upward next to the lower corner of the ice block (light gray in Fig. 1). The ice block distance from the bottom and the left wall of the tank was 2.7 cm. The subglacial discharge freshwater was kept at the freezing temperature of 0°C, and the total flow rate Q_{sg} in the experiments with two sources was kept fixed at 2.26 $cm^3 s^{-1}$, while experiments with a single source had $Q_{sg} = 1.13$ or 2.26 $cm^3 s^{-1}$. The buoyancy flux of the subglacial discharge $B_{sg} = g'_{sg} Q_{sg}$ was 29.8 and 59.6 $cm^4 s^{-3}$ for $Q_{sg} = 1.13$ and 2.26 $cm^3 s^{-1}$, respectively, where $g'_{sg} = g(\rho_{sg} - \rho_2)/\rho_0 = 26.37$ cm s^{-2} is the reduced gravity, g is the gravitational acceleration, ρ_{sg} is the density of the subglacial discharge, ρ_2 is the lower-layer density, and ρ_0 is a reference density. Unless otherwise noted, by "single source" and "single plume," we mean the experiment with $x_0 = 0$ cm and initial flow rate $Q_{sg} = 2.26$ $cm^3 s^{-1}$, and by "two sources" and "two plumes," we mean the experiments with $x_0 > 0$ cm and each source having an initial flow rate of $Q_{sg} = 1.13$ $cm^3 s^{-1}$. The Reynolds number of the flow at the source $\mathrm{Re} = 4Q_{sg}/(\pi d\nu)$ ($\nu = 0.018$ $cm^2 s^{-1}$; the kinematic viscosity of water at 0°C) is 730 for $Q_{sg} = 2.26$ $cm^3 s^{-1}$, and the plume became fully turbulent within 2 or 3 cm from the source. The separation distance between the two sources took the values $x_0 = 2$, 3.9, 5.6, and 7.5 cm.

In the laboratory, the subglacial discharge was represented by a vertical buoyant plume, and we neglect the horizontal momentum that may be forcing the subglacial discharge at the bottom of a glacier. Because of the Coandă effect (Wille and Fernholz 1965), a jet tends to be attracted to a nearby surface. Hence, as observed in numerical simulations (Kimura et al. 2014), the subglacial discharge plumes do not detach from the vertical ice face for realistic levels of discharge. Therefore, we choose to simulate the subglacial discharge plume as a purely vertical plume, with no horizontal momentum, neglecting the small adjustment an oceanic subglacial discharge plume may undergo near the source.

To keep the total water volume constant in the tank, a sink pipe connected to a pump was located at the mouth of the fjord, on the side of the tank opposite the ice block (Fig. 1). The vertical location of the sink was determined by the depth of the intrusion (see section 3), and the pump was set to withdraw water with a flow rate Q_{sg}. A limitation of this experimental setup is the fact that the temperature and salinity of the two layers near the mouth of the fjord cannot be kept constant because the waters of the two layers near the mouth cannot be replenished. The glacially modified water (see section 3) slowly fills up the tank and all experiments terminate when it reaches a depth of 5 cm above the bottom of the tank. The duration of the experiment varied, for different values of x_0 and Q_{sg}, between 30 and 65 min.

The melting of the ice block was measured by weighting the ice block before it was positioned in the tank and at the end of the experiment. The scale used to weight the ice block has an accuracy of 5 g, and we will assume that the uncertainty due to the measurement is ±10 g. The submarine melting rate is defined as

$$\mathrm{smr} = \frac{M_s - M_e}{\rho_i h_i W_i \Delta t}, \tag{1}$$

where M_s and M_e are the weights of the ice block at the start and end of the experiment, respectively; $\rho_i = 0.92\rho_f$ is the density of the ice assumed to be 8% less than that of the freshwater ρ_f used to make the ice block; $h_i = 24.3$ cm is the depth of the ice block immersed in water; and Δt is the duration of the experiment that is known with an uncertainty of ±1 min.

A total of seven experiments with four different values of x_0 were conducted, including two experiments with a single source and two experiments with $x_0 = 2$ cm.

3. Flow circulation

As soon as the subglacial discharge exits the source(s), the dynamics near the ice can be described by the "convection-driven melting" regime (Motyka et al. 2003; Jenkins 2011). In this regime, the primary buoyancy source for the plume(s) is given by the subglacial discharge, with only a small contribution from submarine melting. The subglacial discharge water rises vertically, mixing with the submarine meltwater and with the ambient water entrained by the plume(s). Herein, "glacially modified waters" will refer to the buoyant plume(s) waters that are a combination of subglacial discharge, submarine melting, and entrained ambient waters. The buoyant plume(s) rises until it reaches either the interface between the two layers or the free surface where it intrudes horizontally into the fjord. The depth of intrusion depends on the plume(s) buoyancy forcing (Sciascia et al. 2013). When the glacially modified water intrudes at the interface, a less vigorous plume, forced solely by the submarine melting, rises in the top layer and leaves the ice block at the free surface.

This circulation was previously observed in numerical studies (Sciascia et al. 2013; Xu et al. 2012, 2013) and field studies in Sermilik Fjord (Straneo et al. 2011). These results confirm that the meltwater mainly deposits within the interior of the water column and not entirely at the free surface. When two plumes are present, as they rise vertically they may interact (see section 5)

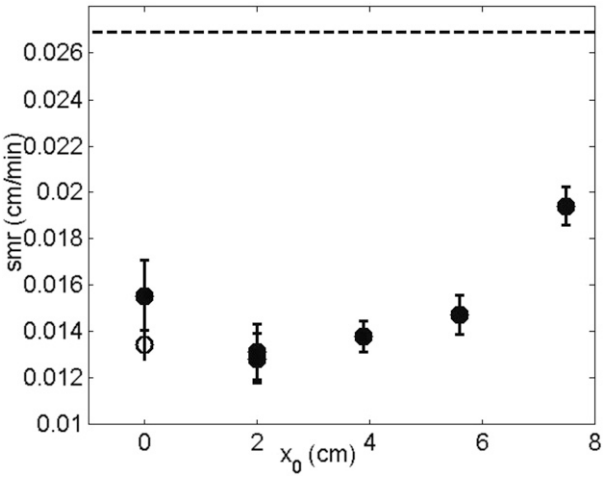

FIG. 2. Submarine melting rate smr as a function of the separation distance between the two sources of subglacial discharge x_0. The total subglacial discharge is $Q_{sg} = 2.26\,\mathrm{cm^3\,s^{-1}}$, and for $x_0 > 0$ cm the initial flow rate of each source is $Q_{sg} = 1.13\,\mathrm{cm^3\,s^{-1}}$. The dashed line indicates twice the melt rate obtained with a single source with an initial flow rate $Q_{sg} = 1.13\,\mathrm{cm^3\,s^{-1}}$. The dashed line is expected to be the melt rate for $x_0 \to \infty$. The open circle indicates the melting for a single source with initial flow rate $Q_{sg} = 1.13\,\mathrm{cm^3\,s^{-1}}$. Error bars are calculated from the uncertainties in the measurement of Δt and the ice block mass.

within the bottom layer if the distance between the sources is approximately $x_0 < H_2\alpha/0.35$, where α is the entrainment constant (Cenedese and Linden 2014; Kaye and Linden 2004).

4. Submarine melting

When two sources of subglacial discharge are present, the submarine melting rate smr is observed to decrease when x_0 increases from $x_0 = 0$ cm (single source) to $x_0 = 2$ cm (two sources), while for $x_0 \geq 2$ cm, the melting monotonically increases with increasing separation distance of the sources x_0 (Fig. 2). For $x_0 \to \infty$, we expect the two buoyant plumes to be independent and the melting to be twice the melting due to a single plume having $Q_{sg} = 1.13\,\mathrm{cm^3\,s^{-1}}$ (open circle; Fig. 2). This value is represented by the dashed line in Fig. 2, but the width of the tank did not allow us to verify the validity of this assumption because for $x_0 > 7.5$ cm the plumes interacted with the sidewalls of the tank and the melting was reduced because of a reduction in entrainment of warm bottom layer waters (not shown). For all experiments with two sources, the two plumes were observed to interact. In particular, albeit only a qualitative measurement, the ice cube at the end of the experiment presented elevated melting above the location of the two sources, and the loss of ice had a conical shape, mimicking the shape of the plumes. These conical shapes in the ice block merged at increasing distance from the bottom for increasing x_0.

5. Discussion

The change in submarine melting rate observed with changing distance between the two sources of subglacial discharge is nonmonotonic: it decreases between $0 \leq x_0 \leq 2$ cm and increases between $2 \leq x_0 \leq 7.5$ cm. The maximum value of melting is expected to occur for two independent plumes, that is, $x_0 \to \infty$ (dashed line, Fig. 2). When the two sources of subglacial discharge are located closer together the two plumes will touch and merge at a distance from the "virtual origin" given by $z_T = 0.35x_0/\alpha$ and $z_M = 0.44x_0/\alpha$, respectively (Cenedese and Linden 2014; Kaye and Linden 2004), where the distance from the virtual origin is $z = (z' + z_V)$, z' is the vertical distance from the source, and z_V is the location of the virtual origin below the source (Hunt and Kaye 2001). The virtual origin correction is necessary because the plume's self-similar solutions of Morton et al. (1956) are strictly valid only for a "pure" plume with zero momentum and volume fluxes. Hence, the virtual origin correction is the distance from the physical source that an imaginary pure plume, with zero momentum and volume fluxes but with the same buoyancy flux issuing from the virtual origin, has in order for the actual buoyancy, momentum, and volume fluxes of the plume to be the same at the physical source. The entrainment of warm bottom layer waters in the two merging plumes is reduced compared to that with two independent plumes (Cenedese and Linden 2014), and as a consequence the plume waters are colder and melting is reduced. As the two sources are located closer together, the two plumes interact for a larger portion of their vertical rise and consequently the melting is reduced for decreasing values of x_0, as shown in Fig. 2.

A different behavior is observed for $0 \leq x_0 \leq 2$ cm that can be explained by looking at the area covered on the ice face by a single plume (Fig. 3a, dotted area) and two merging plumes generated by two sources with a separation distance $x_0 = 2$ cm (Fig. 3a, horizontal lines area). The classic self-similar solutions and entrainment assumption introduced by Morton et al. (1956) can be used to predict the radius of the plume to be $b(z) = (6/5)\alpha z$, when the average buoyancy profile can be represented by a "top hat" profile (Turner 1973). The area covered by a single plume (dashed line, Fig. 3b) is larger than that covered by two merging plumes with $x_0 < 3$ cm (solid line, Fig. 3b); consequently, for $0 \leq x_0 < 3$ cm a single plume is more effective at melting than two merging plumes.

Furthermore, using the self-similar solutions by Morton et al. (1956) for a single plume and the correction

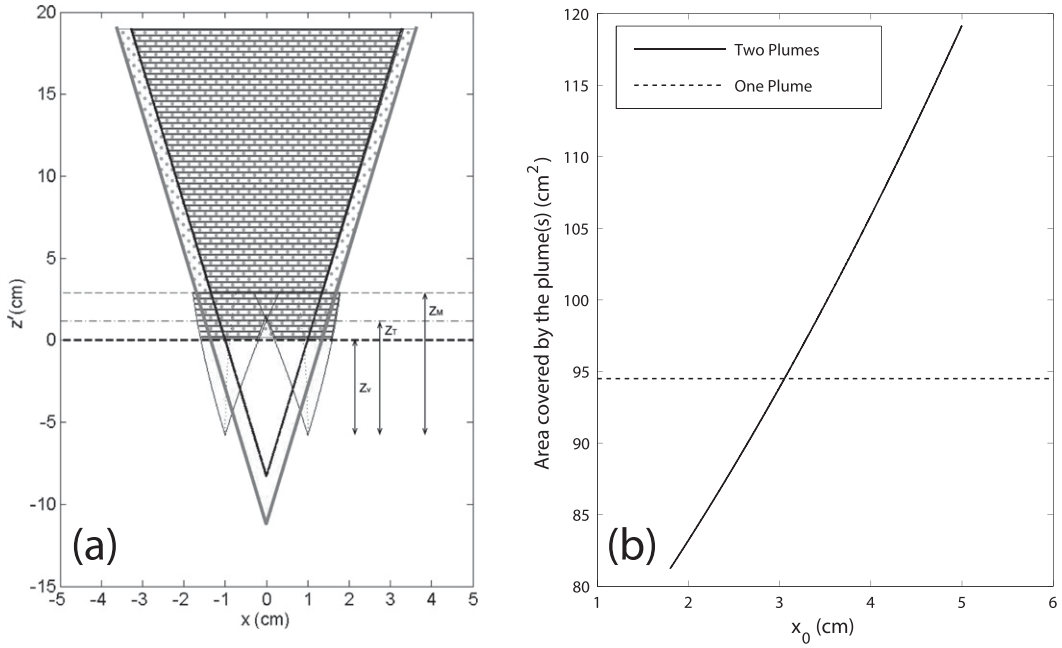

FIG. 3. (a) Area of the ice face covered by a single plume with initial flow rate $Q_{sg} = 2.26\,\mathrm{cm^3\,s^{-1}}$ (dotted area) and by two plumes (horizontal lines area) with sources separated by a horizontal distance $x_0 = 2\,\mathrm{cm}$ and each with an initial flow rate $Q_{sg} = 1.13\,\mathrm{cm^3\,s^{-1}}$. The plumes originate below $z' = 0\,\mathrm{cm}$ because the virtual origin correction has been taken into account. The location of the virtual origin for the two plumes is z_V below the physical origin at $z' = 0\,\mathrm{cm}$. (b) Area covered by a single plume with initial flow rate $Q_{sg} = 2.26\,\mathrm{cm^3\,s^{-1}}$ (dashed line) and by two plumes (solid line) with sources separated by a horizontal distance x_0 and each with an initial flow rate $Q_{sg} = 1.13\,\mathrm{cm^3\,s^{-1}}$.

introduced by Cenedese and Linden (2014) for two interacting plumes, we calculated the amount of warm water entrained into the plume(s). A correction was also introduced to take into account that we are considering only half of a conical plume. The entrainment volume flux $Q_e(z')$ is defined as the entrainment volume flux into the plume(s) occurring between the source ($z' = 0\,\mathrm{cm}$) and the location at a distance z' from the source. Using volume conservation

$$Q_e(z') = \int_0^{z'} \alpha w(z)\pi b(z)\,dz = Q(z') - Q_{sg},$$

where $w(z)$ and $Q(z)$ are the plume(s) vertical velocity and volume flux, respectively, and we used the entrainment assumption to define the entrainment velocity as $w_e(z) = \alpha w(z)$. The entrainment volume flux Q_e into a single plume is larger than that into two plumes when $x_0 \leq 4\,\mathrm{cm}$, while for $6 \leq x_0 \leq 8\,\mathrm{cm}$ Q_e for a single plume is larger than for two plumes only for the first 11 cm from the source(s) (Fig. 4a). Hence, the total entrainment into the two plumes once they reach the interface between the two layers [i.e., $Q_e(z' = 19\,\mathrm{cm})$] is smaller than that into a single plume for $x_0 \leq 4\,\mathrm{cm}$, while that for $6 \leq x_0 \leq 8\,\mathrm{cm}$ is larger (Fig. 4b). For distances larger than $z' = 19\,\mathrm{cm}$, equivalent to considering larger H_2 and taller ice blocks or glaciers, the ratio R of $Q_e(z')$ for two plumes to that of a single plume asymptotically approaches 1 with increasing distances. However, for $x_0 \leq 4\,\mathrm{cm}$, R monotonically increases toward 1, while for $6 \leq x_0 \leq 8\,\mathrm{cm}$, R presents a maximum before monotonically approaching 1 for large integration distances (not shown). The distance from the source(s) at which R is maximum depends on x_0, for the given Q_{sg}.

A larger entrainment volume flux Q_e into the plume(s) is expected to generate a warmer plume(s) and cause larger submarine melting. Hence, the combination of a larger area on the ice face covered by a single plume, for $x_0 < 3\,\mathrm{cm}$, and a larger entrainment volume flux into a single plume, for $x_0 \leq 4\,\mathrm{cm}$, can explain the nonmonotonic behavior of the melt rate observed when two sources of subglacial discharge are present (Fig. 2). For larger values of x_0, the area covered by the two plumes increases with increasing x_0, as well as the entrainment into the two plumes, producing an increase in melt rate with increasing x_0 (Fig. 2). We expect this nonmonotonic behavior to occur also for increasing water depths since Q_e for a single plume is always larger than that into two plumes for $x_0 \leq 4\,\mathrm{cm}$, that is, $R < 1$, and the area of a single plume is always larger than that of two plumes for $x_0 < 3\,\mathrm{cm}$, independent of the integration depth. A similar nonmonotonic dependence of the melt rate with

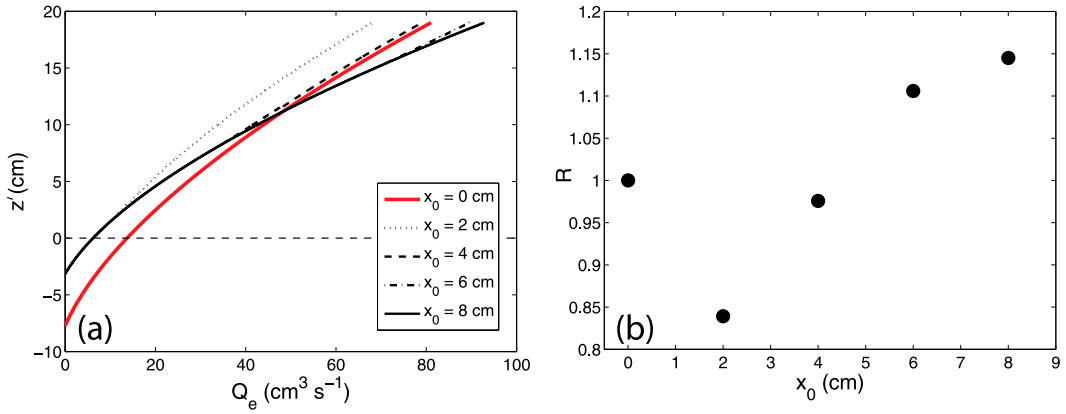

FIG. 4. (a) Entrainment volume flux Q_e as a function of distance from the source z' for a single plume with initial flow rate $Q_{sg} = 2.26\,\mathrm{cm^3\,s^{-1}}$ (red line) and for two plumes (black lines) with sources separated by a horizontal distance x_0 and each with an initial flow rate $Q_{sg} = 1.13\,\mathrm{cm^3\,s^{-1}}$. The plumes originate below $z' = 0$ cm because the virtual origin correction has been taken into account. (b) Ratio R of Q_e for two plumes to that of a single plume, calculated at $z' = 19$ cm, as a function of sources' separation x_0.

x_0 was also observed in the numerical study of Kimura et al. (2014) and was explained qualitatively by the contraction occurring when the two plumes merge, that is, the area on the ice face covered by the plume(s).

6. Conclusions

Buoyant plumes generated by two sources of subglacial discharge rise vertically along the ice face and interact within a layer of depth H_2 if the distance between the sources x_0 is smaller than $H_2\alpha/0.35$. In this study, submarine melting is directly measured and does not depend on parameterizations of unresolved processes. The results suggest that for large separation distances between the interacting plumes the melting increases with distance between the sources as the area of ice face covered by the two plumes increases (Fig. 3b), and the entrainment into two merging plumes increases (Fig. 4a) as the two plumes are located farther apart. However, for small separation distances two factors cause a larger melting for a single plume compared to that of two plumes. The area covered on the ice face by a single plume is larger than that covered by two interacting plumes with $x_0 < 3$ cm (Fig. 3b) and consequently a single plume with initial flow rate Q_{sg} melts more than two interacting plumes each with initial flow rate $Q_{sg}/2$. Furthermore, for $x_0 \leq 4$, the entrainment volume flux into a single plume with initial flow rate Q_{sg} is larger than that into two interacting plumes each with initial flow rate $Q_{sg}/2$. A larger entrainment volume flux causes the single plume to be warmer and melt more than two interacting plumes for small separation distances (Fig. 2). In Sermilik Fjord, subglacial discharge plumes are expected to interact if $x_0 \lesssim 100$ m, and the results of this study have implication both for discharge channels with $x_0 \lesssim 100$ m and for distributed sources for which the discharge is not homogeneous and several localized plumes emerge. In summary, the fact that submarine melting is influenced dramatically by the subglacial discharge means that the discharge details, for example, the numbers and distance of the ''holes'' though which the subglacial discharge water enters the fjord and the water flow rate in each hole, are extremely important and can considerably influence the submarine melting and the fjord stratification and circulation. A better understanding of the small-scale dynamics influencing submarine melting and plume dynamics is therefore necessary to correctly parameterize and represent these processes in numerical models.

Acknowledgments. The authors thank Jason Hyatt and Fiamma Straneo for helpful comments on the manuscript and Anders Jensen for the able assistance in the laboratory. Support to C.C. was given by the NSF Project OCE-1130008 and OCE-1434041. V.M.G. received support from the ''Gori'' Fellowship.

REFERENCES

Bamber, J., M. van den Broeke, J. Ettema, J. Lenaerts, and E. Rignot, 2012: Recent large increases in freshwater fluxes from Greenland into the North Atlantic. *Geophys. Res. Lett.*, **39**, L19501, doi:10.1029/2012GL052552.

Bartholomaus, T. C., C. F. Larsen, and S. O. Neel, 2013: Does calving matter? Evidence for significant submarine melt. *Earth Planet. Sci. Lett.*, **380**, 21–30, doi:10.1016/j.epsl.2013.08.014.

Carroll, D., D. A. Sutherland, E. L. Shroyer, J. D. Nash, G. A. Catania, and L. A. Stearns, 2015: Modeling turbulent subglacial meltwater plumes: Implications for fjord-scale buoyancy-driven circulation. *J. Phys. Oceanogr.*, **45**, 2169–2185, doi:10.1175/JPO-D-15-0033.1.

Cenedese, C., and P. F. Linden, 2014: Entrainment in two coalescing axisymmetric turbulent plumes. *J. Fluid Mech.*, **752**, R2, doi:10.1017/jfm.2014.389.

Church, J. A., and Coauthors, 2011: Revisiting the earth's sea-level and energy budgets from 1961 to 2008. *Geophys. Res. Lett.*, **38**, L18601, doi:10.1029/2011GL048794.

Howat, I. M., I. Joughin, and T. A. Scambos, 2007: Rapid changes in ice discharge from Greenland outlet glaciers. *Science*, **315**, 1559–1561, doi:10.1126/science.1138478.

Hunt, G. R., and N. G. Kaye, 2001: Virtual origin correction for lazy turbulent plumes. *J. Fluid Mech.*, **435**, 377–396, doi:10.1017/S0022112001003871.

Jenkins, A., 2011: Convection-driven melting near the grounding lines of ice shelves and tidewater glaciers. *J. Phys. Oceanogr.*, **41**, 2279–2294, doi:10.1175/JPO-D-11-03.1.

Kaye, N., and P. Linden, 2004: Coalescing axisymmetric turbulent plumes. *J. Fluid Mech.*, **502**, 41–63, doi:10.1017/S0022112003007250.

Kimura, S., P. Holland, A. Jenkins, and M. Piggott, 2014: The effect of meltwater plumes on the melting of a vertical glacier face. *J. Phys. Oceanogr.*, **44**, 3099–3117, doi:10.1175/JPO-D-13-0219.1.

Mortensen, J., K. Lennert, J. Bendtsen, and S. Rysgaard, 2011: Heat sources for glacial melt in a sub-Arctic fjord (Godthåbsfjord) in contact with the Greenland Ice Sheet. *J. Geophys. Res.*, **116**, C01013, doi:10.1029/2010JC006528.

——, J. Bendtsen, R. J. Motyka, K. Lennert, M. Truffer, M. Fahnestock, and S. Rysgaard, 2013: On the seasonal freshwater stratification in the proximity of fast-flowing tidewater outlet glaciers in a sub-Arctic sill fjord. *J. Geophys. Res. Oceans*, **118**, 1382–1395, doi:10.1002/jgrc.20134.

Morton, B. R., G. Taylor, and J. S. Turner, 1956: Turbulent gravitational convection from maintained and instantaneous sources. *Proc. Roy. Soc. London*, **A234**, 1–23, doi:10.1098/rspa.1956.0011.

Motyka, R. J., L. Hunter, K. A. Echelmeyer, and C. Connor, 2003: Submarine melting at the terminus of a temperate tidewater glacier, LeConte Glacier, Alaska, USA. *Ann. Glaciol.*, **36**, 57–65, doi:10.3189/172756403781816374.

——, M. Truffer, M. Fahnestock, J. Mortensen, S. Rysgaard, and I. Howat, 2011: Submarine melting of the 1985 Jakobshavn Isbræ floating tongue and the triggering of the current retreat. *J. Geophys. Res.*, **116**, F01007, doi:10.1029/2009JF001632.

——, W. P. Dryer, J. Amundson, M. Truffer, and M. Fahnestock, 2013: Rapid submarine melting driven by subglacial discharge, LeConte Glacier, Alaska. *Geophys. Res. Lett.*, **40**, 5153–5158, doi:10.1002/grl.51011.

O'Leary, M., and P. Christoffersen, 2013: Calving on tidewater glaciers amplified by submarine frontal melting. *Cryosphere*, **7**, 119–128, doi:10.5194/tc-7-119-2013.

Rignot, E., and P. Kanagaratnam, 2006: Changes in the velocity structure of the Greenland Ice Sheet. *Science*, **311**, 986–990, doi:10.1126/science.1121381.

Sciascia, R., F. Straneo, C. Cenedese, and P. Heimbach, 2013: Seasonal variability of submarine melt rate and circulation in an east Greenland fjord. *J. Geophys. Res. Oceans*, **118**, 2492–2506, doi:10.1002/jgrc.20142.

——, C. Cenedese, D. Nicolí, P. Heimbach, and F. Straneo, 2014: Impact of periodic intermediary flows on submarine melting of a Greenland glacier. *J. Geophys. Res. Oceans*, **119**, 7078–7098, doi:10.1002/2014JC009953.

Shepherd, A., and Coauthors, 2012: A reconciled estimate of ice-sheet mass balance. *Science*, **338**, 1183–1189, doi:10.1126/science.1228102.

Slater, D. A., P. W. Nienow, T. R. Cowton, D. N. Goldberg, and A. J. Sole, 2015: Effect of near-terminus subglacial hydrology on tidewater glacier submarine melt rates. *Geophys. Res. Lett.*, **42**, 2861–2868, doi:10.1002/2014GL062494.

Straneo, F., and P. Heimbach, 2013: North Atlantic warming and the retreat of Greenland's outlet glaciers. *Nature*, **504**, 36–43, doi:10.1038/nature12854.

——, and C. Cenedese, 2015: The dynamics of Greenland's glacial fjords and their role in climate. *Annu. Rev. Mar. Sci.*, **7**, 89–112, doi:10.1146/annurev-marine-010213-135133.

——, G. Hamilton, D. Sutherland, L. Stearns, F. Davidson, M. Hammill, G. Stenson, and A. Rosing-Asvid, 2010: Rapid circulation of warm subtropical waters in a major glacial fjord in east Greenland. *Nat. Geosci.*, **3**, 182–186, doi:10.1038/ngeo764.

——, R. Curry, D. Sutherland, G. Hamilton, C. Cenedese, K. Vage, and L. Stearns, 2011: Impact of fjord dynamics and glacial runoff on the circulation near Helheim Glacier. *Nat. Geosci.*, **4**, 322–327, doi:10.1038/ngeo1109.

——, and Coauthors, 2013: Challenges to understand the dynamic response of Greenland's marine terminating glaciers to oceanic and atmospheric forcing. *Bull. Amer. Meteor. Soc.*, **94**, 1131–1144, doi:10.1175/BAMS-D-12-00100.1.

Turner, J., 1973: *Buoyancy Effects in Fluids*. Cambridge University Press, 367 pp.

Vieli, A., and F. Nick, 2011: Understanding and modelling rapid dynamic changes of tidewater outlet glaciers: Issues and implications. *Surv. Geophys.*, **32**, 437–458, doi:10.1007/s10712-011-9132-4.

Wille, R., and H. Fernholz, 1965: Report on the first European mechanics colloquium, on the Coandă effect. *J. Fluid Mech.*, **23**, 801–819, doi:10.1017/S0022112065001702.

Xu, Y., E. Rignot, D. Menemenlis, and M. Koppes, 2012: Numerical experiments on subaqueous melting of Greenland tidewater glaciers in response to ocean warming and enhanced subglacial runoff. *Ann. Glaciol.*, **53**, 229–234, doi:10.3189/2012AoG60A139.

——, ——, I. Fenty, D. Menemenlis, and M. M. Flexas, 2013: Subaqueous melting of Store Glacier, west Greenland from three-dimensional, high-resolution numerical modeling and ocean observations. *Geophys. Res. Lett.*, **40**, 4648–4653, doi:10.1002/grl.50825.